Available online at www.sciencedirect.com

ScienceDirect

journal homepage: www.elsevier.com/locate/he

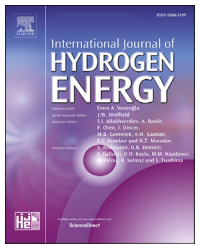

Pt and Pt–Ag nanoparticles supported on carbon nanotubes (CNT) for oxygen reduction reaction in alkaline medium

B. Ruiz-Camacho [a,*], A. Medina-Ramírez [a], R. Fuentes-Ramírez [a], R. Navarro [b], C. Martínez Goméz [b], A. Pérez-Larios [c]

[a] Department of Chemical Engineering, Division of Natural and Exact Sciences, University of Guanajuato, Noria Alta S/n Guanajuato 36050, Mexico

[b] Department of Chemistry, Division of Natural and Exact Sciences, University of Guanajuato, Noria Alta S/n Guanajuato 36050, Mexico

[c] Laboratorio de Investigación en Materiales, Agua y Energía, Departamento de Ingeniería, Centro Universitario de Los Altos, Universidad de Guadalajara, Av. Rafael Casillas Aceves 1200, Tepatitlán de Morelos, Jalisco, 47600, Mexico

HIGHLIGHTS

- Pt and Pt–Ag particles less than 10 nm were supported on CNT by a sonochemical method.
- Pt/CNT exhibits higher electrocatalytic activity for ORR than Pt–Ag/CNT and Pt/C.
- The Pt-CNT interaction improved the electrocatalytic activity towards ORR.
- A small particle size increases the electrochemical active surface of the catalyst.

ARTICLE INFO

Article history:
Received 29 December 2021
Received in revised form
3 March 2022
Accepted 20 March 2022
Available online 16 April 2022

Keywords:
ORR
Alkaline medium
Pt–Ag
Carbon nanotubes
Sonochemical

ABSTRACT

In this work, we investigated the effect of the carbon nanotubes (CNT) as alternative support of cathodes for oxygen reduction reaction (ORR) in alkaline medium. The Pt and Pt–Ag nanomaterials supported on CNT were synthesized by sonochemical method. The crystalline structure, morphology, particle size, dispersion, specific surface area, and composition were investigated by XRD, SEM-EDS, TEM, HR-TEM, N_2 adsorption-desorption and XPS characterization. The electrochemical activity for ORR was evaluated by cyclic voltammetry (CV), linear sweep voltammetry (LSV), and electrochemical impedance spectroscopy (EIS) in alkaline medium. The electrochemical stability was researched by an accelerated degradation test (ADT). Pt/CNT showed the better electrocatalytic activity towards ORR compared with Pt–Ag/CNT and Pt/C. Pt/CNT exhibited higher specific activity (1.12 mA $cm^{-2}{}_{Pt}$) than Pt/C (0.25 mA $cm^{-2}{}_{Pt}$) which can be attributed to smaller particle size, Pt-CNT interaction, and Pt load (5 wt%). The Pt monometallic samples supported on CNT and Vulcan showed higher electrochemical stability after ADT than Pt–Ag bimetallic. The ORR activity of all materials synthesized proceeded through a four-electron pathway. Furthermore, the EIS results showed that Pt/CNT exhibited the lower resistance to the transfer electron compared with conventional Pt/C and Pt–Ag/CNT.

* *Corresponding author.*
E-mail address: beatriz.ruiz@ugto.mx (B. Ruiz-Camacho).

https://doi.org/10.1016/j.ijhydene.2022.03.190

Introduction

The oxygen reduction reaction (ORR) is a cathodic reaction that occurs in fuel cells (FCs). However, ORR exhibits a complex kinetics and needs better electrocatalysts [1]. The main challenge in the development of FCs is the ORR slow kinetic and larger overpotential that has limited the large-scale application [2]. The ORR in alkaline media can involve two parallel pathways (i) Direct four-electron pathway and (ii) Indirect two-electron-pathway, according to the following reactions:

$$O_2 + 2H_2O + 4e^- \leftrightarrow 4OH^- \quad \text{(direct)} \tag{1}$$

$$O_2 + H_2O + 2e^- \leftrightarrow HO_2^- + OH^- \quad \text{(indirect)} \tag{2}$$

$$H_2O + HO_2^- + 2e^- \rightarrow 3OH^- \quad \text{(indirect)} \tag{3}$$

The mechanism and ORR kinetics are highly dependent of several factors such as electrode material (structure, stability, size, etc.) and pH of the electrolyte [3]. The structure characteristics of catalytic surface affects the oxygen adsorption energy and influences in the efficiency of FCs. For accelerating this reaction various electrocatalyst have been developed over the past decades [4]. Pt and Pt-based alloy supported on Vulcan carbon (Pt/C) are currently considered the best electrocatalyst for ORR. Some alloys of Pt with other metals (Fe, Co, Ni, Cu, Ag, Pd) to form Pt-based bimetallic or trimetallic electrocatalysts had also been researched as alternative cathodes for ORR [5]. Specifically, Ag has been considered as a promising replacement of Pt for ORR in alkaline medium due to it is abundantly available in nature, has a relatively low price, good methanol tolerance and acceptable catalytic activity [2,6]. Deng et al. [7] reports that the incorporation of other metals like Ag in the Pt-based modifies the Pt surface electronic structure increasing its electrochemical activity for ORR. Additional reports of the use Ag in cathodes for ORR indicate an improvement in the electrocatalytic activity for ORR compared with Pt/C. Pt–Ag nanotubes prepared by a controlled galvanic technique exhibit an extraordinary ORR activity in acid medium showing 4.5 times higher than Pt/C catalysts [8]. According to Esfandiari et al. [9], Ag@Pt/C (1:3) core-shell electrocatalysts show stability and its ORR activity proceeded through a 4 e^- reaction pathway. Furthermore, in alkaline medium, several reports indicated that the use of silver catalyst can improve the catalytic activity for ORR, for example, CNTs-Ag/MnO_2 [2], Ag/C [4], Pt-Ag [10], Ag/B-MWCNTs [11], and Ag/MWNTs [12]. Additionally, Ag exhibits enhanced electrocatalytic performance due to it provides oxygen-containing species to remove CO adsorbed on Pt, improving the poisoning resistance ability of platinum [13,14].

Carbon nanotubes (CNTs), carbon nanofibers (CNFs), carbon aerogels and graphene nanoplates have been researched as new supports of metallic particles to improve the stability, uniform distribution, reduce metal particle size, and diminish the metal loading [15]. Specifically, CNTs are considered as one of the best choices due to it has high surface area, thermal conductivity, chemical stability, electrical and ionic conductivity, and ease for availability, which makes it a suitable candidate as support of Pt and Pt–Ag for fuel cell applications [16,17]. Several reports in the literature using CNT as a support for fuel cells indicated that the unique morphology and one-dimensional structure provides good electron transfer and higher electrical conductivity [15]. Also, CNT doped with phosphorus as support of Pt can promote a low Pt loading and good electrocatalytic activity for ORR in acidic medium [18]. The functionalization of CNTs with carboxyl functional groups and nitrogen or indazole groups had also been reported for ORR in PEM fuel cells [15]. Additionally, the doped carbons materials as either metal-free catalyst have been one of the recent topics in the catalysts of fuel cell for ORR [19]. For example, reports of bimetallic and trimetallic samples like Fe–Co, FeNi, Co_9S_8@Co embedded or implanted in nitrogen-doped carbon materials show excellent ORR features in alkaline medium [20–22].

In the present study, the preparation of electrodes-based Pt on CNTs were performed as an alternative support to increase the electrochemical activity of Pt for ORR in alkaline medium. Pt and Pt–Ag nanoparticles were successfully synthesized by sonochemical method. The effect of support (Vulcan/CNT) and composition Pt and Pt–Ag on the electrochemical properties for ORR was investigated. The as prepared Pt catalysts showed that Pt/CNT exhibits better properties for ORR compared with conventional Pt/C and Pt–Ag/CNT due to the small Pt particle size, composition and higher dispersion obtained.

Experimental methodology

Chemicals

Chloroplatinic acid hexahydrate ($H_2PtCl_6 \cdot 6H_2O$), silver nitrate ($AgNO_3$) and isopropyl alcohol (C_3H_8O) for the synthesis of Pt and Pt–Ag nanoparticles were purchased from Sigma Aldrich. The substrates were commercial samples: carbon Vulcan XC72R (Fuel Cell Store), and open carbon nanotubes (Sigma Aldrich). 5 wt% solution of Nafion, and potassium hydroxide 85% (KOH) for the electrochemical test were purchased from Sigma Aldrich. Distilled water was used as solvent.

Materials preparation

Pt/CNT, Pt–Ag/CNT, and Pt/C electrocatalysts were synthesized by sonochemical method using a theoretical 10 wt% metal load [23]. Bimetallic sample was prepared by using a mass ratio (1:2) of Pt–Ag supported on CNT. Briefly, 50 mL of $H_2PtCl_6 \cdot 6H_2O$ solution (1×10^{-3} M) was mixed with 50 mL of isopropyl alcohol. The carbon support (Vulcan XC 72R or CNT) was added to the Pt solution under sonication for 5 h at room temperature and nitrogen atmosphere, using an ultrasonic bath (42 kHz). The solvent was removed by evaporation all night recovering the precipitate. In the case of Pt–Ag/CNT, the bimetallic nanomaterial was prepared with 25 mL of $AgNO_3$ solution, mixed with a platinum alcoholic solution at the same concentration, and following the same sonochemical methodology described. An illustration of the synthesis methodology is presented in Fig. 1.

Structural characterizations

The crystalline phases presented on the supports and electrocatalysts were identified by X-ray diffraction (XRD) using a PANalytical Model Empyrean diffractometer. Textural properties (surface area, pore volume, and pore size) were determined by nitrogen adsorption-desorption with a Micromeritics (TriStar II Plus, Norcross, GA, USA). The samples were degassed at 200 °C for 2 h under a vacuum. Nitrogen adsorption isotherms were measured at liquid nitrogen temperature (77 K) with nitrogen pressures ranging from 10 to 6 to 1.0 P/P0. The specific surface area was obtained by the Brunauer–Emett–Teller method (BET) and the pore size distribution following the Barret–Joyner–Halenda (BJH) method. The morphology of samples synthesized was investigated by scanning electron microscopy (SEM) analysis using a field emission scanning electron microscope Zeiss® Sigma HD VP. The elemental composition was determined by EDS using a JEOL scanning electron microscope (model JSV-6610LV). The particle size and metal dispersion were analyzed by transmission electron microscopy (TEM) using a JEOL 1010 transmission electron microscope operated at 80 kV. High resolution TEM images (HRTEM) were obtained by using a transmission electron microscopy (Jeol, JEM ARM200F, Boston, MA USA) operated at 200 kV. The X-ray photoelectron spectroscopy (XPS) analysis (K-Aplha + TM X-ray photoelectron spectrometer system-Thermo Scientific) was performed to determine the chemical state of the platinum deposited on the supports and the elemental analysis of the electrocatalysts. The analyses were carried out by using a Kα radiation of 1486.6 eV. The binding energy (BE) shift was corrected with reference to the C1s BE (284.8 eV).

Electrochemical characterization

The electrochemical activity of Pt/CNT, Pt–Ag/CNT, and Pt/C towards ORR in alkaline medium was investigated at room temperature by cyclic voltammetry (CV) and linear sweep voltammetry (LSV) techniques using a conventional three-electrode cell connected to a Gamry Instruments potentiostat/galvanostat. A glassy carbon electrode (0.196 cm^2), a graphite bar, and a saturated calomel electrode (SCE = 0.24 V vs NHE) were used as the work, counter, and reference electrodes, respectively [24]. All potentials were referred to the reversible hydrogen electrode (RHE). The catalytic ink was prepared with 3 mg of catalyst, 400 μL of isopropyl alcohol and 2.0 μL of Nafion solution (5 *wt* %). This suspension was sonicated for 1 h, and 10 μL of the ink were deposited on the surface of working electrode (0.38 mg cm^{-2} was the net load of catalysts on the gassy carbon electrode). Before the ORR test, 30 cycles of CV were performed to stabilize the current-potential signal in nitrogen atmosphere at 50 mV s^{-1}. The potential range of CV used in alkaline electrolyte was from 0.05 to 1.2 V/RHE. The LSV was obtained using a rotating disk electrode (RDE) in alkaline electrolyte saturated with oxygen at different rotating rated (200, 400, 900, and 1600 rpm) at scan rate of 5 mV s^{-1}. An electrochemical stability test was performed by cycling between 0.6 and 1.0 V for 2000 cycles in the O_2-saturated 0.5 M KOH solution at scan rate of 50 mVs^{-1}. Cyclic voltammetry in N_2 atmosphere as well as a LSV at 900 rpm in O_2 saturated alkaline electrolyte was obtained before and after 2000 cycles [25]. Additionally, electrochemical impedance spectroscopy (EIS) was employed to evaluate the catalysts in terms of their charge transfer resistance. EIS experiments were performed at potential of E = 0.92V/RHE, after a pre-polarization at the same potential for 120 s. During the EIS analysis, the working electrode was rotating at 1000 rpm. The amplitude of the signal perturbation was 100 mV and the frequency range from 20 kHz to 10 mHz.

Results and discussion

Characterization

Fig. 2 (a) shows the XRD results of Pt/C, Pt/CNT and Pt–Ag/CNT in the range of 2θ between 10 and 80°. The face-centered cubic (fcc) structure of Pt was observed around 39.9°, 46.2° and 67.5° of 2θ values correspond to the (1 1 1), (2 0 0), and (2 2 0) planes in three samples synthesized (JCPDS No. 4–802). Pt–Ag/CNT diffraction peaks presented a downshift of the Pt peaks to lower diffraction angles compared with Pt monometallic catalysts, for example, in the pattern of Pt–Ag/CNT, the peak of plane (1 1 1) is near 2theta = 39.2° compared with Pt pure (39.9°). According to literature, this effect can be attributed to the incorporation of Ag atom into Pt metallic structure in the

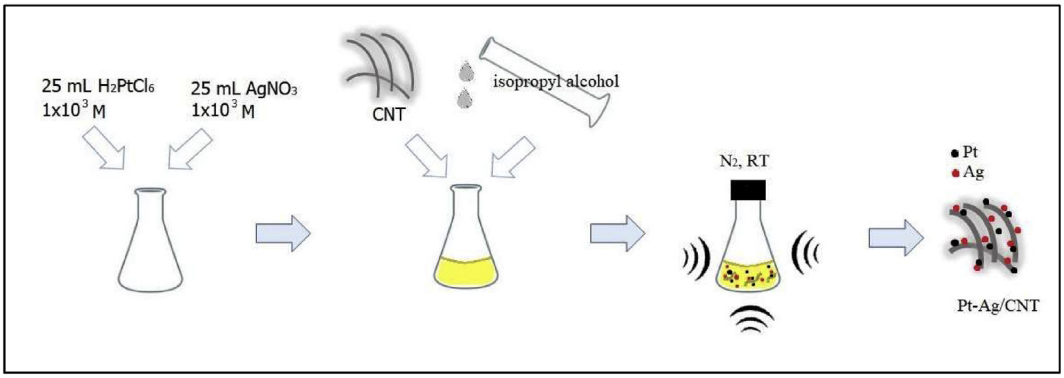

Fig. 1 – Illustration of the synthesis of Pt–Ag/CNT by chemical reduction using sonochemical method at RT in nitrogen atmosphere.

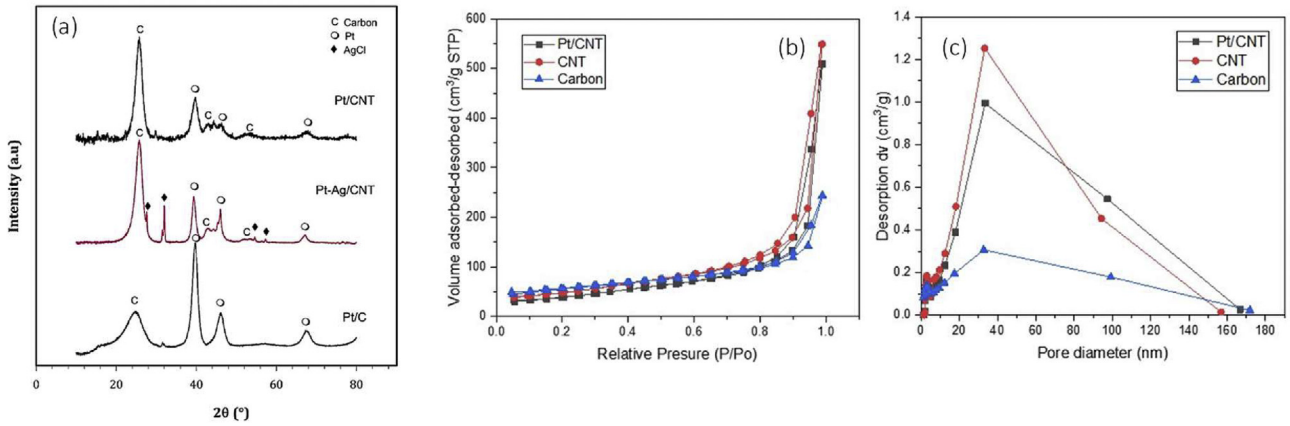

Fig. 2 – (a) XRD results, (b) N_2 adsorption-desorption isotherms and (c) the pore-diameter distribution plot of Pt/CNT, Pt–Ag/CNT and Pt/C electrocatalysts prepared by sonochemical method.

Pt–Pt lattice distance [25–28]. The peak around 25.75° corresponds to the diffraction (002) plane of the carbon, which is observed with higher intensity in the catalysts supported on CNT compared with Pt/C. The peaks at 43°, 53.5°, and 77.3° are associated with (1 0 0), (0 0 4) and (1 0 0) graphite structure, respectively [29]. Additionally in the Pt–Ag/CNT others peaks around to 27°, 32°, 54° and 57° of 2θ were detected, they corresponded to the AgCl crystals (JCPDS No. 31–1238). Similar findings were reported by Duok et al. [30], they indicated that the formation of AgCl is due to the galvanic replacement reaction between metallic silver and platinum ions. The presence of AgCl has been associated with the formation of the bimetallic catalysts [31].

The crystallite size of nanoparticles was calculated based on the reflection from the main (1 1 1) crystallographic plane by using Scherrer equation [15]. Table 1 shows that the Pt–Ag/CNT (13.7 nm) bimetallic sample exhibits higher crystallite size compared with monometallic Pt/CNT (8.1 nm) and Pt/C (10.1 nm). Similar results of higher crystal size in silver electrodes compared with platinum are reported in the literature [7,9,24,27].

The pore structure of a carbon support reflected the capability of the water transport property of Pt structure for cathode side of the PEMFC. That means that the support with a high surface area and large pore volume is desired as well as excellent electrical conductivity [9].

Fig. 2 (b) shows the adsorption/desorption isotherms obtained by nitrogen physisorption for the supports (Vulcan and CNT) and Pt/CNT. Results indicated that the three materials exhibited an isotherm type III, this characteristic is indicative of weak interactions between the adsorbate and the adsorbent. Furthermore, the monolayer density is unequally distributed on the most active areas [32]. The Vulcan support (189 $m^2\ g^{-1}$) have a higher specific surface area than CNT (172 $m^2\ g^{-1}$). The lower specific surface area of Pt/CNT (142 $m^2\ g^{-1}$) indicated that various Pt nanoparticles were accumulated inside of some pores of CNT. Similar specific surface area for supports have been reported by others [33]. Furthermore, an increase in the adsorption volume is observed in inverse order to the value of the specific area. In Fig. 2 (c) was observed that the materials have a monomodal pore diameter distribution that goes from 1 to 169 nm, which can effectively promote the mass transport during the catalysis process [22].

Table 1 – Physical and electrochemical properties of catalysts synthesized by sonochemical method.

Electrocatalyst	Pt/CNT	Pt–Ag/CNT	Pt/C
Crystal size (nm)	8.1	13.7	10.1
Particle size (nm)	5.44	8.25	4.11
% wt[a]	5.5	1.2:0.99	6.4
% wt[b]	5.9	1:0.44	7.8
Pt(0) 4_{f7} (eV)	71.12	72.73	71.07
Pt(II) 4_{f7} (eV)	71.84	71.13	71.61
ECSA ($m^2\ g^{-1}_{Pt}$)	26.9	–	122.01
n	3.8	3.4	3.5
$E_{1/2}$ (V)	0.080	0.008	0.072
Tafel slope (mV dec^{-1})	−100	−68	−66
j_k at 0.9 V(mA cm^{-2}_{geo})	1.06	0.406	0.99

[a] EDS results.
[b] XPS analysis.

The morphology and elemental composition of Pt/CNT, Pt–Ag/CNT, and Pt/C were investigated by SEM micrographs and EDS (Fig. 3 and Table 1). The morphology of CNT was clearly distinguished from spherical form of Vulcan carbon by SEM images, the CNT are several micrometers in length compared to Vulcan. EDS results demonstrated that the Pt nominal content for Pt/C and Pt/CNT was 6.4 and 5.5 wt%, respectively. The bimetallic sample showed a composition for Ag and Pt of 1.2 and 0.99 wt%, respectively. These results demonstrated that the nominal metal is lower than theoretical value (10 wt%), which can be related to the synthesis method as well as the growth of Pt nanoparticles that depends on the physical properties of supports (textural, structural, morphology or functional surface groups) [34].

Fig. 4 displays the TEM and particle size distribution histograms of samples prepared. Metallic particles of Pt and Pt–Ag in a spherical morphology distributed onto the different support were observed. Pt/C and Pt/CNT monometallic samples exhibited a higher dispersion compared with Pt–Ag/CNT bimetallic sample. Table 1 reports the particle size results

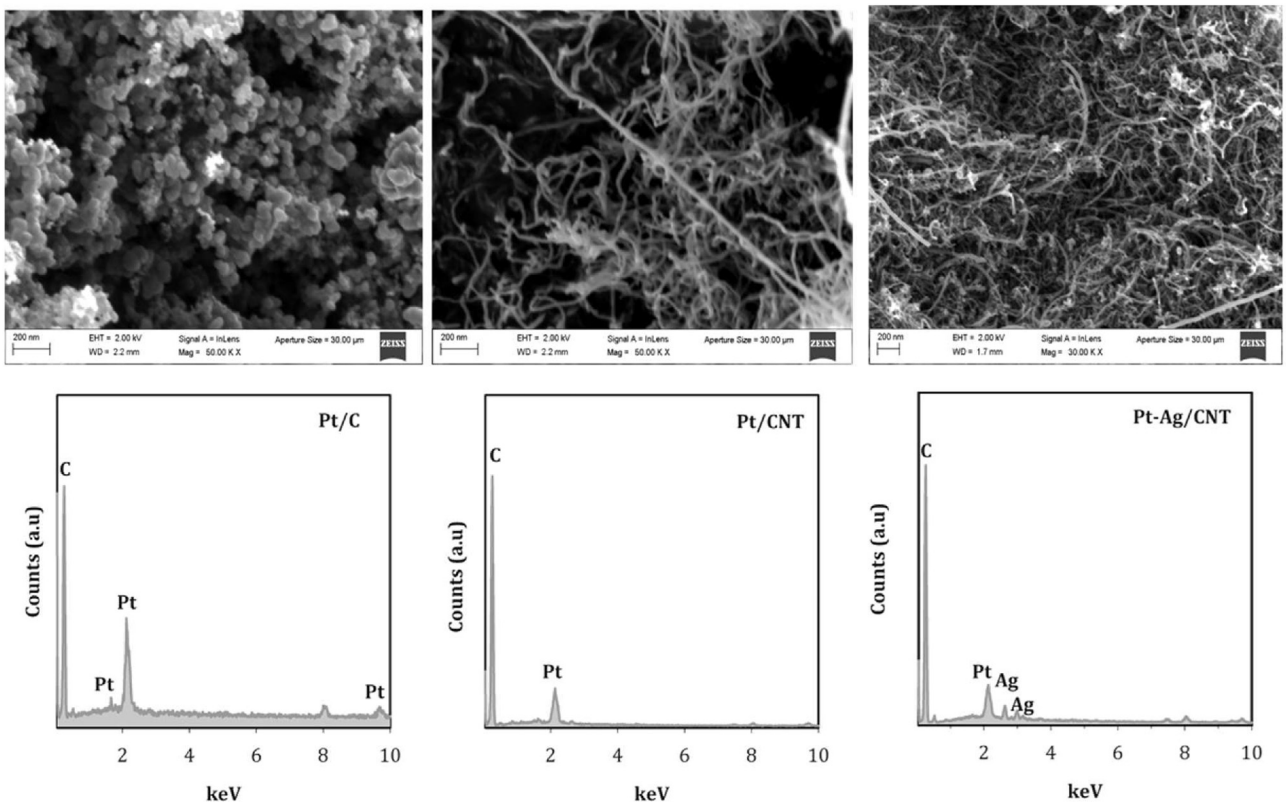

Fig. 3 – SEM micrographs and EDS analysis of Pt/CNT, Pt–Ag/CNT and Pt/C electrocatalysts prepared by sonochemical method.

indicating that monometallic samples Pt/C and Pt/CNT present a smaller particle size compared with Pt–Ag/CNT. The Pt and Pt–Ag particle size follow the same tendency than the crystallite size calculated by Scherrer equation. These TEM results means that the presence of Ag nanoparticles favors the aggregation of metal particles. Similar results are reported by others, who indicated that it is still a challenge to control the size distribution and avoid the aggregation of the Ag nanoparticles, especially in the case of ultra-high Ag loading on carbon supports [4]. According to literature, Ag has similar lattice constant matching with Pt, this feature can facilitate the growth of Pt–Ag alloy which possesses remarkable thermodynamic stability [35]. Also, the Ag–Pt nanoparticles present several advantages: there is a reduction of the poisoning effect; catalytic properties are improved; silver –base nanoparticles are competitive alternative to Pt [36]. Moreover, the relevance of study AgPt nanoparticles for electrocatalysis is because that they exhibit strong electronic producing a strong enhancement of catalytic activity [37]. Additionally, in this work the Pt and Pt–Ag nanoparticles prepared by sonochemical method are smaller than 10 nm.

Fig. 5 shows the high-resolution TEM (HRTEM) images collected from Pt/CNT, Pt–Ag/CNT and Pt/C. The interplanar spacing's of Pt is 0.22 nm that corresponds to (1 1 1) lattice plane of face-centered cubic (FCC) structure founded in Pt/CNT as well as Pt/C. CNT showed a lattice spacing of 0.34 nm that corresponds to (0 0 2) lattice plane of graphite of carbon nanotube [2,8,25,38]. According to literature Ag nanoparticles can exhibit an interplanar spacing of 0.21, 0.12, 0.132, and 0.223 nm which are assigned to the (2 0 0), (3 1 1), (1 1 1) and (2 2 0) lattice planes of FCC structure [39]. Due to Ag has similar lattice constant matching with Pt, this feature can facilitate the growth of a core-shell structure of Ag–Pt nanoparticles forming agglomerates of up to 100 nm as it is observed in Fig. 5 [9,35].

The XPS results of platinum (Pt_{4f}) region for samples prepared Pt/CNT, Pt–Ag/CNT and Pt/C are shown in Fig. 6. XPS analysis were carried out to evaluate the surface composition and valence state of the samples. XPS results were reported in Table 1. Three electrocatalysts shows the signals correspond to metallic and oxidized platinum. The Pt 4f peaks are analyzed by deconvolution and the curves involve three doublets, each one can be ascribed to the dominant metallic Pt (0), Pt(II) of $Pt(OH)_2$ and Pt(IV) species [26]. The Pt_{4f} peaks of Pt/CNT (71.12 eV) presented a positive shift compared with Pt/C (71.07 eV) which can be associated with the interaction Pt-support. According to literature a positive shift of binding energy suggest that the d-band center of Pt moves downwards, which will reduce the binding strength of oxygenated species producing an increase of ORR activity [25]. Also, this positive shift is associated to a decrease in the electronic charge density of the Pt atoms due to Pt-support interactions [32,40]. The presence of Pt oxide was observed around 71.13 eV (Pt–Ag/CNT), 71.61 eV (Pt/C) and 71.84 eV (Pt/CNT), which coincides with that reported in the literature [32]. The Pt_{4f} peaks of Pt–Ag/CNT (72.73 eV) shows a more positive shifts compared to Pt/C and Pt/CNT, which can be related with the electronic interaction effect of bimetallic nanostructures [8].

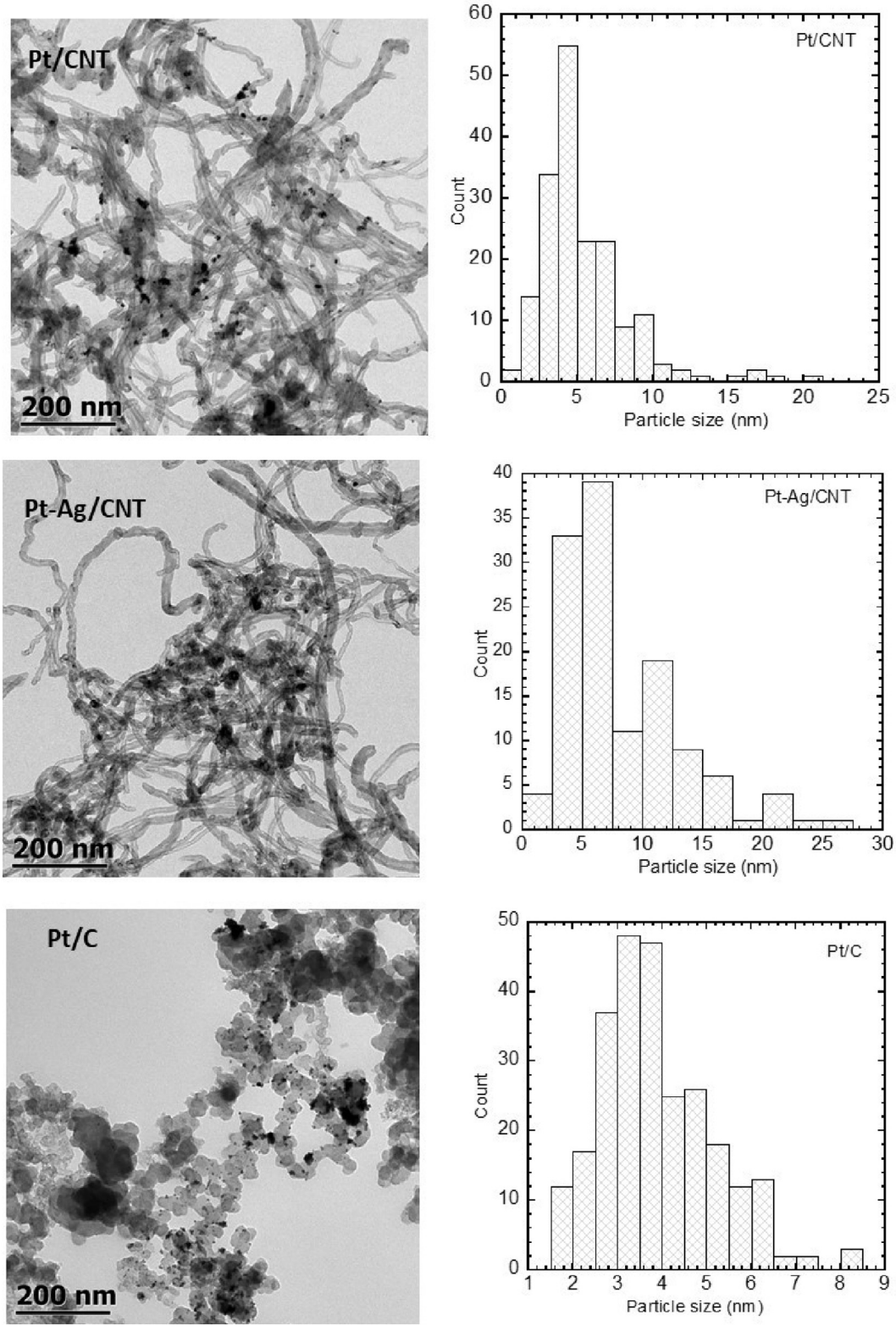

Fig. 4 – TEM and particle size distribution histograms of Pt/CNT, Pt–Ag/CNT and Pt/C.

The Ag 3d spectra of bimetallic sample show a binding energy of 379.98 eV (Ag $3d_{3/2}$) and 367.2 eV (Ag $3d_{5/2}$) which can be associated to Ag (I) [41]. XPS mass percentage analysis confirmed that Pt content in bimetallic sample is lower than monometallic catalysts: Pt–Ag/CNT (1:0.44%) < Pt/CNT (5.9%) < Pt/C (7.8%). These percentage load determinated by XPS are agreed with EDS results (Table 1). These findings are related to the metallic-support interactions which are strongly dependent on the composition and intrinsic properties of the supports.

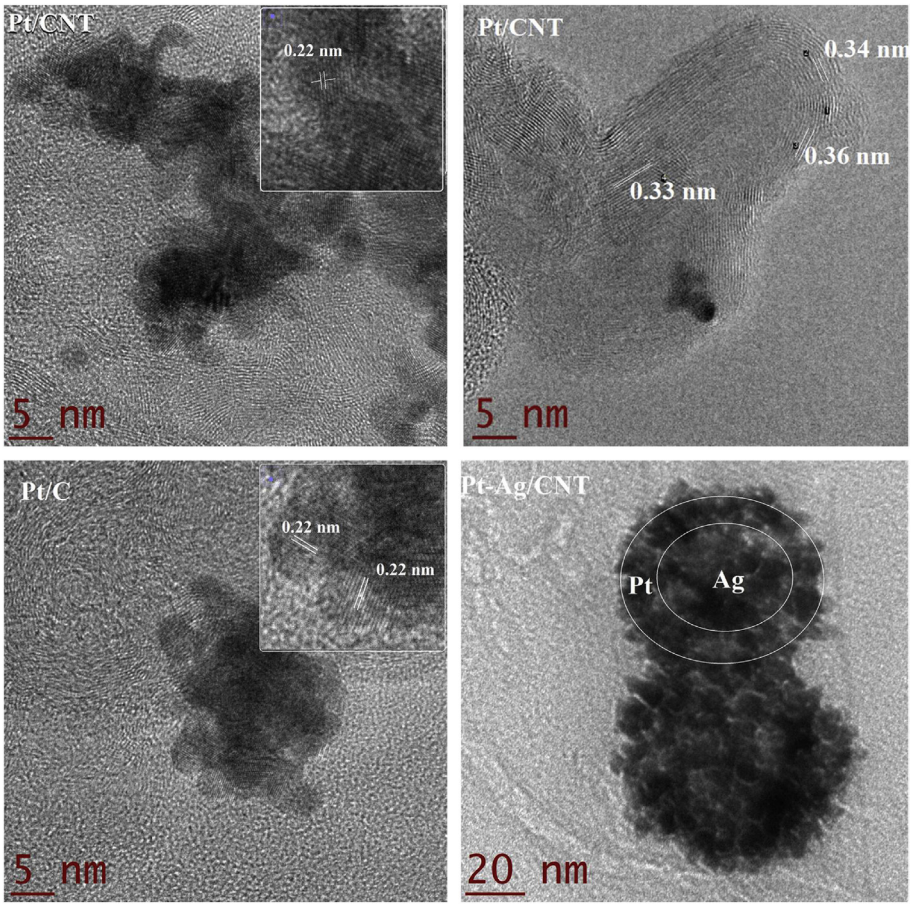

Fig. 5 – HRTEM images of Pt/CNT, Pt–Ag/C and Pt/C electrocatalysts synthesized by sonochemical method.

Electrochemical performance

Fig. 7 (a) presents the CV curves of Pt and Pt–Ag materials synthesized and tested in N_2-saturated 0.5 M KOH solution at scan rate of 50 mV s^{-1} at room temperature. The materials prepared exhibited the typical fingerprint of Pt nanoparticles in alkaline medium which is characterized by the hydrogen adsorption/desorption on the Pt surface ascribed to the current peaks between 0.05 and 0.3 V/RHE, the double layer appears in the range 0.4–0.6 V/RHE, and the adsorption of hydroxyl species (OH_{ads}) on the catalysts surfaces takes place in the range of 0.7–1.2 V/RHE [10]. The hydrogen adsorption-desorption region is smaller in the Pt/CNT compared with Pt/C, which can be related to the Pt particle size, metal dispersion and lower Pt load onto the support. In the case of Pt–Ag/CNT the region of hydrogen is not well defined which can be attributed to low loading of Pt-Ag according to EDS results.

Fig. 7 (a) was used to determine the electrochemical active surface area (ECSA) data of Pt. The ECSA (cm^2mg^{-1}) = $Q/[(0.210)(m)(\upsilon)]$, where the Q (C) is the coulombic charge, 0.210 mC m^{-2} represents the charge required to oxidize a monolayer of H_2 and is used as the conversion factor, m is the amount of Pt on the electrodes obtained from the chemical composition (mg), and υ the scan rate (0.05 V s^{-1}) [42]. Table 1 shows the ECSA values obtained for Pt/C (122.01 m^2/g) was higher than Pt/CNT (26.9 m^2/g). Similar ECSA data of Pt electrocatalysts for ORR are reported by others [4,7–9,25,28]. According to literature, higher ECSA indicates that Pt/C has the largest number of available active sites for oxygen adsorption [7]. In the case of Pt–Ag/CNT the ECSA value was not calculated due to the hydrogen adsorption-desorption region is not well defined which is associated with a poor Pt–Ag load and dispersion.

Fig. 7 shows the ORR polarization curves obtained on (b) Pt/CNT, (c) Pt–Ag/CNT and (d) Pt/C in oxygen saturated 0.5 M KOH by using different rotation rates (ω). The LSV curves obtained are characterized by three regions, I) the kinetic region, where the current (i_k) is independent of the rotating rate; (II) the mixed control region, where both kinetic and mass transfer phenomena occur; III) the mass transfer region, where the diffusion limiting current, i_d, depends on the rotation rate, which means that the limiting current density increases with the increasing rotation rate [19]. However, in the case of the Pt–Ag/CNT sample (Fig. 7 c) the limiting current plateau corresponding to the diffusion-limited current density is not well defined at 900 and 1600 rpm, which can be related with the low Pt–Ag load.

To further comparing the ORR electrocatalytic activity of electrocatalysts studied, Fig. 8 (a) displays the LSV of samples synthesized at same rotating rate of 900 rpm. Results clearly show that the ORR in the activation region is more favorable on Pt/CNT electrocatalyst, and it shows the more positive

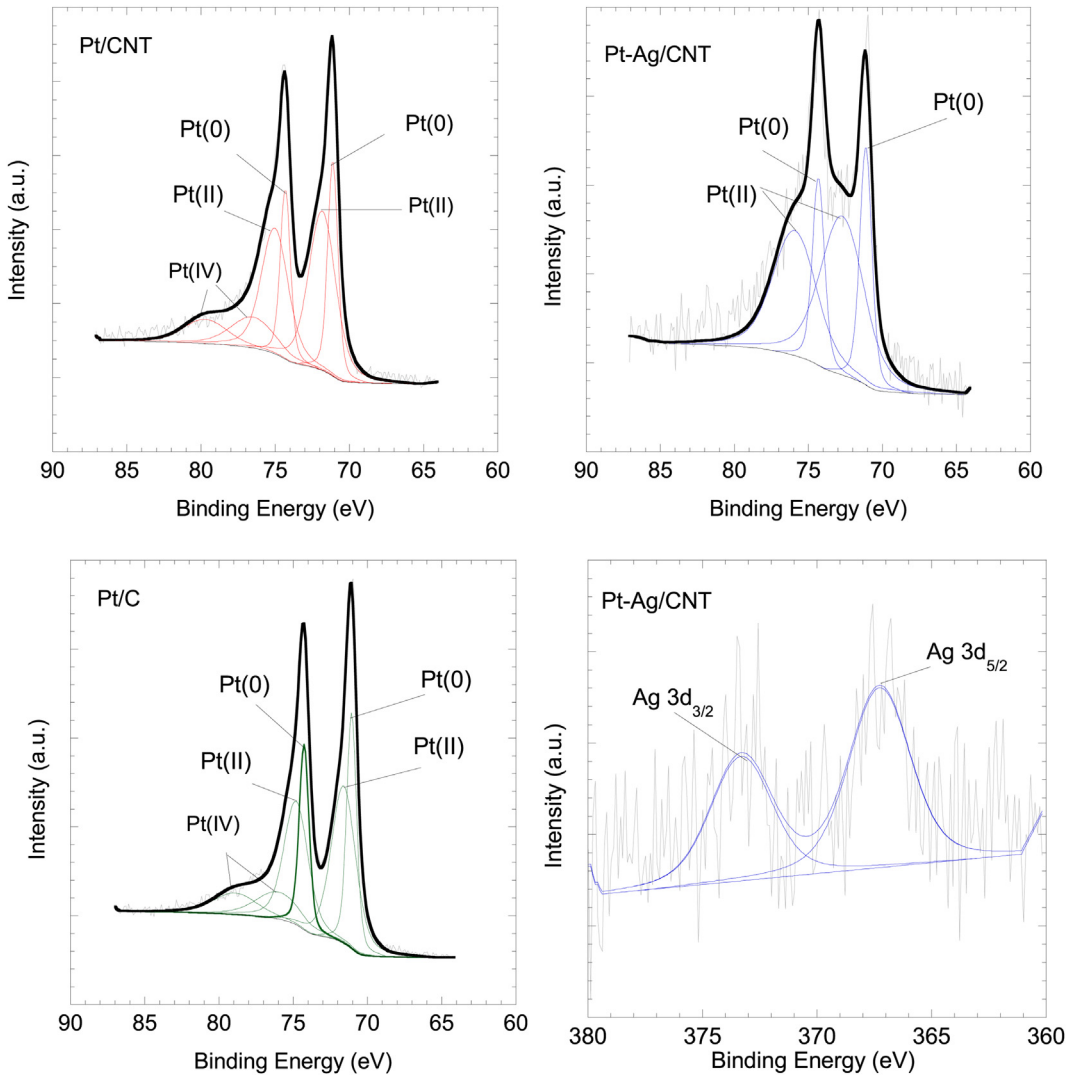

Fig. 6 – High-resolution Pt 4f spectra of Pt/CNT, Pt–Ag/CNT and Pt/C electrocatalyst and Ag 3d spectra of bimetallic Pt–Ag/CNT sample.

onset-potential compared with the Pt/C and Pt–Ag/CNT. The most positive half wave potential ($E_{1/2}$) of Pt/CNT (0.08 V) demonstrated superior activity for ORR than Pt/C (0.072 V) and Pt–Ag/CNT (0.008V). These results are related to the small Pt particle size, higher dispersion, Pt load and Pt-CNT interaction compared with Pt–Ag/CNT. As it is well known, electrocatalytic ORR in alkaline medium is a multi-electro reaction that has two main possible pathways: one direct of two electrons to product ion peroxide HO_2^- and other involving a direct four-electron route to produce OH^- (Eqs. (1)–(3)) [8]. The number of electrons transfer during the ORR process on RDE for samples prepared were estimated by the Koutecky-Levich (K-L) Eq. (4):

$$\frac{1}{j}=\frac{1}{j_k}+\frac{1}{j_d}=\frac{1}{j_k}+\frac{1}{0.2nFD^{2/3}\upsilon^{-1/6}C\omega^{-1/2}} \quad (4)$$

where 0.2 is a constant used when ω (rotating rate of the electrode) is expressed in rpm; *n*, the number of electrons transferred during the ORR process; *F*, the Faraday constant (96,485C mol^{-1}); *D* (1.93×10^{-5} cm^2 s^{-1}) and *υ* (0.01 cm^2 s^{-1}) are the diffusion component and the kinematic viscosity, respectively. *C* (1.26×10^{-6} mol cm^{-3}) is the concentration of dissolved oxygen and ω is the rotation speed (rpm) [3,11,21,39]. Using these parameters, a series of K–L plot (j^{-1} vs. $\omega^{-1/2}$) at different potentials (0.3, 0.4, 0.5, 0.6 V/RHE) were obtained for each catalyst. Fig. 8 (b) shows the K-L at 0.4 V/RHE for Pt/CNT, Pt–Ag/CNT, and Pt/C. The Pt/CNT (10.96 mA^{-1} $rpm^{-1/2}$), Pt–Ag/CNT (12.25 mA^{-1} $rpm^{-1/2}$) and Pt/C (11.9 mA^{-1} $rpm^{-1/2}$) catalysts showed a similar K-L comparable with the theoretical value (10.7 mA^{-1} rpm $^{-1/2}$) [43]. The average number of electrons transferred estimated (*n*) were 3.8, 3.4, and 3.5 for Pt/CNT, Pt–Ag/CNT, and Pt/C, respectively. These results are close to 4.0, which means that the process of ORR in alkaline medium on Pt/CNT is preferential undergone by direct four-electron pathway to produce OH^- ($O_2 + 2H_2O + 4e^- \leftrightarrow 2OH^-$) [10].

Fig. 8 (c) displays the Tafel plot deduced after mass transfer correction of LSV results. The Tafel slope obtained for Pt/CNT,

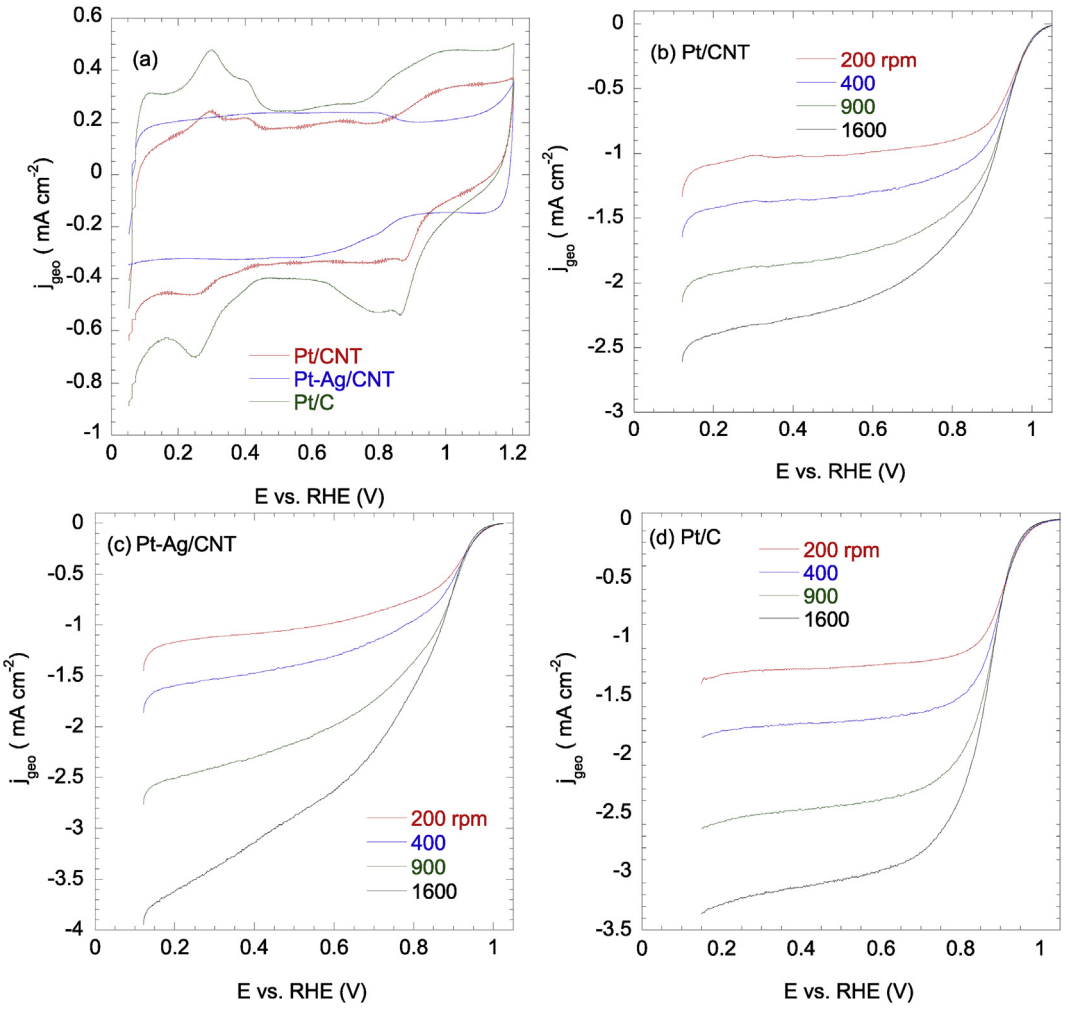

Fig. 7 – (a) Cyclic voltammetry of Pt and Pt–Ag materials prepared by sonochemical method. N_2 atmosphere in KOH 0.5 M electrolyte at scan rate of 50 mV s^{-1}. RDE polarization curves of (b) Pt/CNT, (c) Pt–Ag/CNT and (d) Pt/C in O_2-saturated 0.5 M KOH electrolyte with a scan rate of 5 mVs^{-1}.

Pt–Ag/CNT, and Pt/C were −100, −68, and −66 mV dec^{-1}, respectively. According to literature the Tafel slope of −60 mV dec^{-1} corresponds to a pseudo two-electron reaction as the rate determining step (RDS), whereas Tafel slope of −120 mV dec^{-1} suggests the first-electron reduction reaction of oxygen as RDS [2,4,24,44,45]. Table 2 shows the specific (mA $cm^{-2}{}_{Pt}$) and mass (mA mg^{-1}) activities calculated at 0.9 V/RHE for materials prepared. The specific activity results showed that Pt/CNT (1.12 mA $cm^{-2}{}_{Pt}$) is 4 times more active than Pt/C (0.25 mA $cm^{-2}{}_{Pt}$), respectively. These results are related to the smaller Pt particle size, higher metal dispersion, Pt load and Pt-CNT interaction compared with Pt/C and Pt–Ag/CNT. Additionally, the unique properties of CNT as support of Pt (surface area, conductivity, and stability) improved the ORR activity of Pt in alkaline electrolyte. Similar specific and mass activities for Pt, Ag and Pt–Ag electrodes are reported by others in alkaline as well as acid electrolytes (Table 2).

An accelerating durability test (ADT) was realized with a continuously scanning for 2000 cycles in nitrogen atmosphere at 50 mV s^{-1}. Fig. 8 (d), (e), and (f) shows the comparison of the CVs obtained before and after 2000 cycles for materials synthesized. In the case of Pt/CNT and Pt/C samples their CV curves didn't exhibits significant changes, which confirms the electrochemical stability of Pt monometallic samples prepared by the sonochemical method as simple and economical method. However, the bimetallic sample (Pt–Ag/CNT) exhibited a deactivation of the material showing a reduction in the current density along the CV signal after 2000 cycles. Pt–Ag/CNT deactivation can be related with the synthesis methodology used, the core-shell structure obtained and weak bimetallic interaction with the support. Which is controversial with the report of Fu et al. [25] whose report reveal that Pt–Ag sample possesses better electrochemical stability than the commercial Pt/C after the ADT test by 15000 cycles. Similar ADT results were presented by Den et al. [7], they report that after ADT of 5000 cycles the Pt–Ag shows an increase of the ECSA compared with Pt/C that showed aggregation and dissolution of the Pt nanoparticles. Also, Zhan et al. [8] found that Pt–Ag nanotubes supported on carbon show stability after 10000 cycles with negligible activity decay. Furthermore, Fig. 7 (g), (h), and (i) displays the LSV curves for the ORR at 900 rpm in O_2 atmosphere before and after 2000

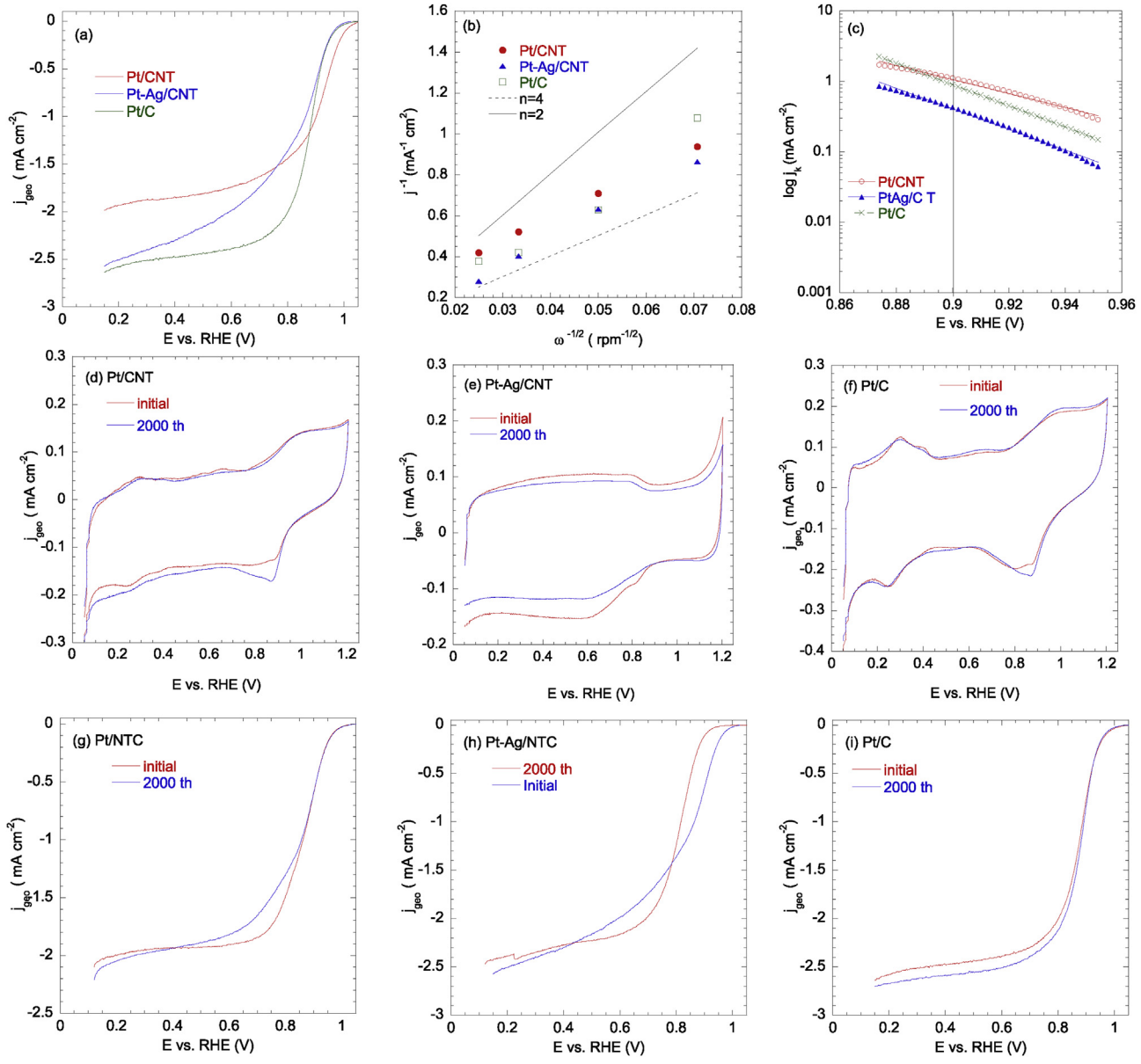

Fig. 8 – (a) ORR comparison at 900 rpm, (b) Koutecky-Levich plots at 0.4 V/RHE and (c) Tafel slopes of samples prepared in KOH 0.5 M. CVs before and after 2000 cycles of (d) Pt/CNT, (e) Pt–Ag/CNT and (f) Pt/C in N_2 saturated KOH 0.5 M at 20 mV s^{-1}. LSV curves at 900 rpm before and after 2000 cycles at 5 mV s^{-1}.

cycles. LSV results confirmed higher electrochemical stability of Pt/CNT and Pt/C compared with Pt–Ag/CNT sample after 2000 cycles. As a conclusion the synthesis method to prepare Pt–Ag/CNT should be improved to increase the stability of Pt–Ag.

The Nyquist and Bode plots obtained from impedance study of ORR on Pt samples prepared are showed in Fig. 9. The EIS analysis was performed for the synthesized electrocatalyst at a frequency range from 20 kHz to 0.01 Hz in the kinetic region (E = 0.9 V/RHE) to obtain the transfer electron resistance. Fig. 8 (a) shows the Nyquist diagrams obtained for Pt/CNT, Pt–Ag/CNT and Pt/C results showed features similar in all samples that correspond to the electrochemical capacitor features [46]. According to the zoom of the Nyquist diagram (inserted in Fig. 8a), apparently the bimetallic catalyst exhibits a higher resistance to the electrolyte. According to Nyquist plot, Pt/CNT presents the lower resistance to the transfer electron compared with conventional Pt/C, and Pt–Ag/CNT.

The Bode plot presents that the phase angle is close to 90° in the low frequency region at potential of 140 mV which can be fitted with the equivalent circuit (EC) proposed in the inset of Fig. 9 (b). The EC corresponds to a series combination of solution resistance (R1) and a parallel arrangement between R2 and CPE, where R2 represent mass transfer resistance at high potential and CPE1 (constant phase element) represents the electrode-electrolyte interfacial capacitance, which can be related to the surface inhomogeneity, roughness, reactivity, porosity, and electrode geometry [47]. However, for obtained the quantitative values of the components of EC, the

Table 2 – Specific and mass activity at 0.9 V/RHE for Pt and Ag electrodes for ORR.

Electrocatalysts	Specific activity at 0.9 V (mA cm^{-2}_{Pt})	Mass activity at 0.9 V (A mg^{-1})	reference
Pt/CNT	1.12	0.30	This work
Pt/C	0.25	0.31	This work
Pt–Ag/C	–	0.24	Fu et al., 2017 [25]
Pt/C	0.07	0.05	Den et al., 2020 [7]
Pt_1Ag_2	0.12	0.10	Den et al., 2020 [7]
Pt/C	–	0.39	Chen et al., 2013 [24]
Ag/m-MWCNTs	–	0.11	Chen et al., 2013 [24]
PtAg-2	0.3125	0.3125	Zhang et al., 2018 [8]
Pt/C	0.25	0.167	Zhang et al., 2018 [8]
Ag	0.16	–	Tammeveski et al., 2012 [12]
AgNP/MWCNTs	0.21	–	Tammeveski et al., 2012 [12]

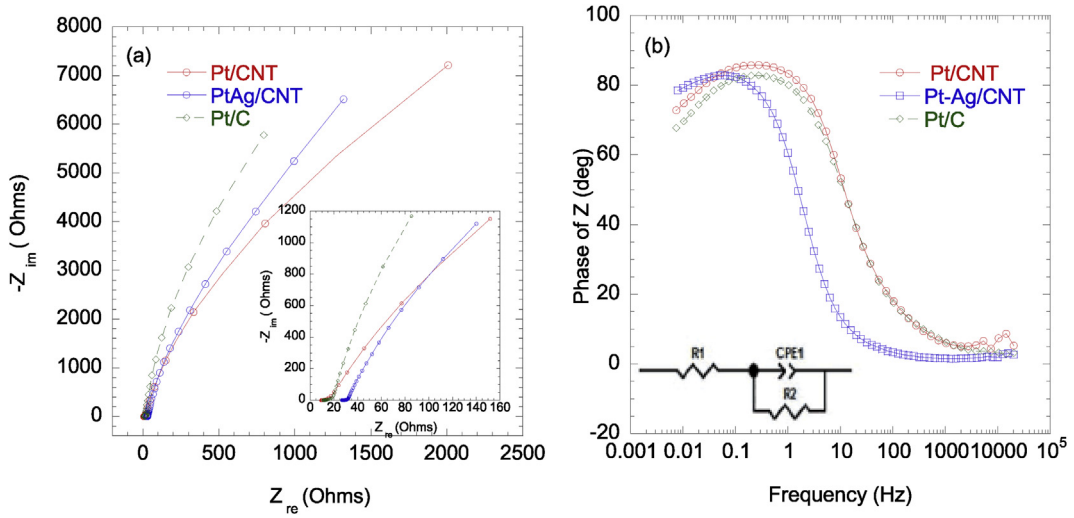

Fig. 9 – (a) Nyquist diagrams and (b) Bode plot of the ORR on Pt/CNT, Pt–Ag/CNT and Pt/C in O_2 saturated solution of alkaline medium at 1000 rpm and 0.90 V/RHE of potential.

experimental impedance data should be fitting EIS data with the electrical circuit proposed, which will be analyzed in a future work.

Conclusion

Pt–Ag and Pt nanoparticles (<10 nm) supported on CNT were successfully synthesized by sonochemical synthesis, and their electrocatalytic activity for ORR in alkaline medium was investigated and compared with conventional Pt/C. The sonochemical method to prepare metal nanoparticles presented several advantages like since is carried out at room temperature, no special equipment, or thermal treatment are required after or during the electrocatalysts preparation. Pt monometallic samples showed a smaller Pt particle and crystallite size, higher dispersion and metal load compared with Pt–Ag bimetallic material. Electrochemical results revealed that Pt/CNT showed higher electrochemical activity for ORR in alkaline medium, lower onset potential, higher half wave potential and favors the 4-electrons transference for the ORR, which is related to the Pt-CNT interaction obtained that favored the electron transference and improved the kinetic to catalyze the ORR. Pt monometallic samples showed better electrochemical stability after 2000 cycles compared with Pt–Ag bimetallic. This research provided a facile method of synthesis of monometallic Pt nanoparticles with higher ORR catalytic activity.

Declaration of competing interest

The authors declare that they have no known competing financial interests or personal relationships that could have appeared to influence the work reported in this paper.

Acknowledgments

The authors are grateful for University of Guanajuato (Project 54/2022) and CONACyT (project INFR-2015-01-254944). We also thanks to Palma-Tirado L. of the UNAM for TEM analysis, Guanajuato University-CONACYT National Laboratory for SEM analysis and E. Medina of the English revision.

REFERENCES

[1] Du C, Sun Y, Shen T, Ying T, Zhang J. 7- Applications of RDE and RRDE methods in oxygen reduction reaction. Chapter 7. Elsevier; 2014. p. 231–77.

[2] Li Z, Zhang J, Lin L, Luo S, Meng A, Song G, et al. Carbon nanotubes-supported Ag/MoO_2 or Ag/MnO_2 heterostructures for a highly efficient oxygen reduction reaction. Mater Char 2021;176:111147–56.

[3] Kiani M, Tian XQ, Zhang W. Single atom based electrocatalysts for oxygen reduction reaction in polymer electrolyte membrane fuel cell: recent advances, challenges, and future perspectives. J Phys Chem Solids 2021;153:109989.

[4] Xu X, Tan C, Liu H, Wang F, Li Z, Liu J, et al. Carbon black supported ultra-high loading silver nanoparticle catalyst and its enhanced electrocatalytic activity towards oxygen reduction reaction in alkaline medium. J Electroanal Chem 2013;696:9–14.

[5] Cruz-Martínez H, Rojas-Chavez H, Matadamas-Ortiz PT, Ortiz-Herrera JC, Lopez-Chávez E, Solorza-Feria O, et al. Current progress of Pt-based ORR electrocatalysts for PEMFCs; an integrated view combining theory and experiment. Materials Today Physics 2021;19:100406.

[6] Truong VM, Duong NB, Yang H. Comparison of carbon supports in anion exchange membrane fuel cells. Materials 2020;13:5370–82.

[7] Deng X, Yin S, Sun M, Zhang S, Xuan W, Xie Z. Shape-tunable Pt-Ag nanocatalysts with excellent performance for oxygen reduction reaction. Int J Hydrogen Energy 2020;45:16482–8.

[8] Zhang E, Ma F, Liu J, Sun J, Chen W, Rong H, et al. Porous platinum-silver bimetallic alloys; surface composition and strain tunability towards enhanced electrocatalysis. Nanoscale 2018;10:21703–11.

[9] Esfandiari A, Kazemeini M, Bastani D. Synthesis, characterization and performance determination of an Ag@Pt/C electrocatalyst for the ORR in a PEM fuel cell. Int J Hydrogen Energy 2016;41:20720–30.

[10] Liu Q, He Y-M, Weng X, Wang AJ, Yuan P-X, Fang K-M, et al. One-pot aqueous fabrication of reduced graphene oxide supported porous PtAg alloy nanoflowers to greatly boost catalytic performance for oxygen reduction and hydrogen evolution. J Colloid Interface Sci 2018;513:455–63.

[11] Cheng Y, Tian Y, Tsang S-W, Yan C. Ag nanoparticles on boron doped multiwalled carbon nanotubes as synergistic catalysts for oxygen reduction reaction in alkaline media. Electrochim Acta 2015;174:919–24.

[12] Tammeveski L, Erickson H, Sarapuu A, Kozlova J, Ritslaid P, Sammelselg V, et al. Electrocatalytic oxygen reduction on silver nanoparticle/multi-walled carbon nanotube modified glassy carbon electrodes in alkaline solution. Electrochem Commun 2012;20:15–8.

[13] Fen JJ, Lin XX, Chen LX, Liu MT, Yuan J, Wang AJ. Ionic liquid-assisted synthesis of composition-tunable cross-linked AgPt aerogels with enhanced electrocatalysis. J Colloid Interface Sci 2017;48:22–30.

[14] Sharma G, Kumar D, Kumar A, Al-Muhtaseb AH, Pathania D, Naushad M, et al. Revolution from monometallic to trimetallic nanoparticle composites, various synthesis methods and their applications: a review. Mater Sci Eng C 2017;71:1216–30.

[15] Litkohi HR, Bahari A, Gatabi MP. Improved oxygen reduction reaction in PEMFCs by functionalized CNTs supported Pt-M (M = Fe, Ni, Fe-Ni) bi- and tri-metallic nanoparticles as efficient electrocatalyst. Int J Hydrogen Energy 2020;45:23543–56.

[16] Ning L, Liu X, Deng M, Huang Z, Zhu A, Zhang Q, et al. Palladium-based nanocatalysts anchored on CNT with high activity and durability for ethanol electro-oxidation. Electrochim Acta 2019;297:206–14.

[17] Ashok A, Kuma A, Yuda A, Ashraf AA. Highly efficient methanol oxidation reaction on durable Co9S8 @N, S-doped CNT catalyst for methanol fuel cell applications. Int J Hydrogen Energy 2022;47:3346–57.

[18] Liu Z, Shi Q, Zhang R, Wang Q, Kang G, Peng F. Phosphorus doped carbon nanotubes supported low Pt loading catalyst for the oxygen reduction reaction in acidic fuel cells. J Power Sources 2014;268:171–5.

[19] Zhao H, Xing T, Li L, Geng X, GueoKe, Sun C, et al. An B, Synthesis of cobalt and nitrogen co-doped carbon nanotubes and its ORR activity as the catalyst used in hydrogen fuel cells. Int J Hydrogen Energy 2019;44:25180–7.

[20] Han Z, Lin S-Y, Feng J-J, Zhang L, Zhang Q-L, Wang A-J. Transitional metal alloyed nanoparticles entrapped into the highly porous N-doped 3D honeycombed carbon: a high-efficiency bifunctional oxygen electrocatalyst for boosting rechargeable Zn-air batteries. Int J Hydrogen Energy 2021;46:19385–96.

[21] Meng H-L, Lin S-Y, Fen J-J, Zhang L, Wang A-J. Coordination regulated pyrolysis synthesis of ultrafine FeNi/$(FeNi)_9S_8$ nanoclusters/nitrogen, sulfur-codoped graphitic carbon nanosheets as efficient bifunctional oxygen electrocatalysts. J Collid Interface Sci 2022;610:573–82.

[22] Sun R-M, Feng J-J, Fang K-M, Wang A-J. In situ produced Co9S8 nanoclusters/Co/Mn-S, N multi-doped 3D porous carbon derived from eriochrome black T as an effective bifunctional oxygen electrocatalyst for rechargeable Zn-air batteries. J Colloid Interface Sci 2022;608:2100–10.

[23] Ruiz Camacho B, Martínez Álvarez O, Rodríguez Santoyo HH, López Pérez PA, Fuentes Ramírez R. Mono and bi-metallic electrocatalyst of Pt and Ag for oxygen reduction reaction synthesized by sonication. Electrochem Commun 2015;61:5–9.

[24] Cheng Y, Li W, Fan X, Liu J, Xu W, Yan C. Modified multi-walled carbon nanotube/Ag nanoparticle composite catalyst for the oxygen reduction reaction in alkaline solution. Electrochim Acta 2013;111:635–41.

[25] Fu T, Huang J, Lai S, Zhang S, Fang J, Zhao J. Pt skin coated hollow Ag-Pt bimetallic nanoparticles with high catalytic activity for oxygen reduction reaction. J Power Sources 2017;365:17–25.

[26] Yang Z, Wang X, Kang X, Zhang S, Guo Y. The PtPdAg/C electrocatalyst with Pt-rich surfaces via electrochemical dealloying of Ag and Pd for ethanol oxidation. Electrochim Acta 2017;236:72–81.

[27] Ruiz-Camacho B, Medina-Ramírez A, Fuentes-Ramírez R, Claudia M, Gómez. Simple synthesis of Pt-Ag/SnO_2-C for use as a catalyst of methanol oxidation in alkaline media. J Solid State Electrochem 2017;21:2449–56.

[28] Ruiz-Camacho B, Morales-Rodríguez R, Medina-Ramírez A. Pt-Ag/C catalyst for methanol oxidation and alcohol tolerant cathode in different electrolytes. Int J Hydrogen Energy 2016:23336–44.

[29] López Tinoco J, Lara Romero J, Rangel R, Apolinar-Cortés J, Paraguay-Delgado f, Jiménez-Sandoval S, et al. Microwave-assisted synthesis of ceria nanoparticles on carbon nanotubes and their dye-removal assessment. J Mater Res Technol 2021;13:70–82.

[30] Duok AS, Saravani H, Noroozifar M. One-pot synthesis of ultrasmall Pt-Ag nanoparticles decorated on graphene as a high-performance catalyst toward methanol oxidation. Int J Hydrogen Energy 2018;43:7946–55.

[31] Peng C, Hu Y, Liu M, Zheng Y. Hollow raspberry-like PdAg alloy nanospheres: high electrocatalytic activity for ethanol oxidation in alkaline media. J Power Sources 2015;278:69–75.

[32] Pérez-Díaz PJ, Medina-Ramírez A, Galindo Esquivel IR, García Ruiz C, Ruiz Camacho B. Effect of X zeolite-carbon composite ratio as support of Pt nanoparticles for MOR and ORR. Ionics 2021;27:1813–28.
[33] Peigney A, Laurent Ch, Flahaut E, Bacsa RR, Rousset A. Specific surface area of carbon nanotubes and bundles of carbon nanotubes. Carbon 2001;39:507–14.
[34] Lee WJ, Bera S, Kim CM, Koh EK, Hong WP, Oh SJ, et al. Synthesis of highly dispersed Pt nanoparticles into carbon supports by fluidized bed reactor atomic layer deposition to boost PEMFC performance. NPG Asia Mater 2020;12:40.
[35] Li Z, Li Y, He C, Shen PK. Bimetallic PtAg alloyed nanoparticles and 3-D mesoporous graphene nanosheets hybrid architectures for advanced oxygen reduction reaction electrocatalysts. J Mater Chem A 2017;5:23158–69.
[36] Ko WY, Su JW, Guo CH, Lin KJ. Extraordinary mechanical flexibility in composite thin films composed of bimetallic AgPt nanoparticle-decorated multiwalled carbon nanotubes. Carbon 2012;50:2244–51.
[37] Vasilva A, Haschke S, Mikhailovskii V, Gitlina A, Bachmann J, Manshina A. Direct laser-induced deposition of AgPt@C nanoparticles on 2D and 3D substrates for electrocatalytic glucose oxidation. Nano-Struct. Nano-Objects 2020;24:100547.
[38] Arteaga G, Rivera-Gavidia LM, Martínez SJ, Rizo R, Pastor E, García G. Methanol oxidation on graphemic-supported platinum catalysts. Surfaces 2019;2:16–31.
[39] Roy N, Ejaz A, Jeon S. Increasing the number of active its of polymer-assisted carbon nanotubes/Ag nanopaticles for enhanced oxygen reduction. Appl Surf Sci 2022;578:151973–86.
[40] Sen F, Gokagac G. Different sized platinum nanoparticles supported on carbon: an XPS study on these methanol oxidation catalysts. J Phys Chem C 2007;111:5715–20.
[41] Adam AMM, Deng M, Zhu A, Zhang Q, Liu Q. Facile one-step room temperature synthesis of PdAg nanocatalysts supported on multi-walled carbon nanotubes towards electro-oxidation of methanol and ethanol, vol. 339; 2020. p. 135929–40.
[42] Doña Rodriguez JM, Herrera Melian JA, Pérez Peña J. Determination of the real surface area of Pt electrodes by hydrogen adsorption using cyclic voltammetry. J Chem Educ 2000;77:1195–7.
[43] Masa J, Batchelor-McAuley C, Schuhman W, Compton RG. Koutecky-Levich analysis applied to nanoparticle modified rotating disk electrodes: electrocatalysis or misinterpretation. Nano Res 2013;7(1):71–8.
[44] Santos LGRA, Freitas KS, Ticianelli EA. Heat treatment effect of Pt-V/C and Pt/C on the kinetic of the oxygen reduction reaction in acid media. Electrochim Acta 2009;54:5246–51.
[45] Ge X, Sumboja A, Wu D, An T, Li B, Thomas Goh FW, et al. Oxygen reduction in alkaline media: form mechanisms to recent advances of catalysts. ACS Catal 2015;5:4643–67.
[46] Singh RK, Devivaraprasad R, Kar T, Chakraboty A, Neergat M. Electrochemical impedance spectroscopy of oxygen reduction reaction (ORR) in a rotating disk electrode configuration: effect of ionomer content and carbon-support. J Electrochem Soc 2015;162:F489–98.
[47] Hirschorn B, Orazem ME, Tribollet B, Vivier V, Frateur I, Musiani M. Determination of effective capacitance and film thickness from constant-phase-element parameters. Electrochim Acta 2010;55:6218–27.